PHYSICAL REVIEW D **90,** 112002 (2014)

Measurement of *CP* violation parameters in $B^0 \to DK^{*0}$ decays

R. Aaij *et al.*[*]
(LHCb Collaboration)

(Received 31 July 2014; published 2 December 2014)

An analysis of $B^0 \to DK^{*0}$ decays is presented, where D represents an admixture of D^0 and $\bar{D}^0$ mesons reconstructed in four separate final states: $K^-\pi^+$, π^-K^+, K^+K^- and $\pi^+\pi^-$. The data sample corresponds to 3.0 fb^{-1} of proton-proton collision, collected by the LHCb experiment. Measurements of several observables are performed, including *CP* asymmetries. The most precise determination is presented of $r_B(DK^{*0})$, the magnitude of the ratio of the amplitudes of the decay $B^0 \to DK^+\pi^-$ with a $b \to u$ or a $b \to c$ transition, in a $K\pi$ mass region of ± 50 MeV$/c^2$ around the $K^*(892)$ mass and for an absolute value of the cosine of the K^{*0} helicity angle larger than 0.4.

DOI: 10.1103/PhysRevD.90.112002 PACS numbers: 14.40.Nd

I. INTRODUCTION

Direct *CP* violation can arise in $B^0 \to DK^{*0}$ decays from the interference between the two color-suppressed $b \to u$ and $b \to c$ transitions shown in the Feynman diagrams of Fig. 1, when the D^0 and $\bar{D}^0$ mesons decay to a common final state. Here and in the following, D represents a neutral meson that is an admixture of D^0 and $\bar{D}^0$ mesons and K^{*0} represents the $K^*(892)^0$ meson. Inclusion of charge conjugate processes is implied unless specified otherwise.

The amount of *CP* violation is related to the value of the weak phase

$$\gamma \equiv \arg\left(-\frac{V_{ud}V_{ub}^*}{V_{cd}V_{cb}^*}\right), \tag{1}$$

the least well determined angle of the unitarity triangle, where V_{ij} are elements of the Cabibbo-Kobayashi-Maskawa (CKM) matrix [1]. The current experimental measurements are $\gamma = (72.0^{+14.7}_{-15.6})^\circ$ by the LHCb Collaboration [2], $\gamma = (69^{+17}_{-16})^\circ$ by the *BABAR* [3] Collaboration and $\gamma = (68^{+15}_{-14})^\circ$ by the Belle Collaboration [4]. This angle can be measured with extremely small theoretical uncertainties [5], using decay modes proceeding through amplitudes involving only the exchange of a W boson. Such methods to determine γ from hadronic B-decay rates were originally proposed in Refs. [6,7] for $B \to DK$ decays and can be applied to the $B^0 \to DK^{*0}$ decay [8]. In this decay, the charge of the kaon from the $K^{*0} \to K^+\pi^-$ decay unambiguously identifies the flavor of the decaying B meson. Hence, no flavor tagging is needed.

The use of these specific neutral B meson decays is interesting since the interfering amplitudes are of comparable size, as opposed to the charged $B^+ \to DK^+$ decay that involves both color-suppressed and color-allowed amplitudes; hence the system could exhibit larger *CP*-violating effects. Contributions from B^0 decays to the $DK^+\pi^-$ final state through non-K^{*0} intermediate resonances can pollute the DK^{*0} reconstructed signal candidates because of the large natural width of the K^{*0}. They are treated following Ref. [9], with the use of a coherence factor, κ, in addition to the hadronic parameters r_B and δ_B, defined as

$$\kappa \equiv \left| \frac{\int |A_{cb}(p)A_{ub}(p)| e^{i\delta(p)} \mathrm{d}p}{\sqrt{\int |A_{ub}(p)|^2 \mathrm{d}p \int |A_{cb}(p)|^2 \mathrm{d}p}} \right|, \tag{2}$$

$$\delta_B \equiv \arg\left(\frac{\int |A_{cb}(p)A_{ub}(p)| e^{i\delta(p)} \mathrm{d}p}{\sqrt{\int |A_{ub}(p)|^2 \mathrm{d}p \int |A_{cb}(p)|^2 \mathrm{d}p}} \right), \tag{3}$$

$$r_B \equiv \sqrt{\frac{\int |A_{ub}(p)|^2 \mathrm{d}p}{\int |A_{cb}(p)|^2 \mathrm{d}p}}, \tag{4}$$

where $A_{ub}(p)$ and $A_{cb}(p)$ are the amplitudes of the $b \to u$ and $b \to c$ transitions, respectively, to the $B^0 \to DK^+\pi^-$ decays, $\delta(p)$ is the strong-phase difference between the two

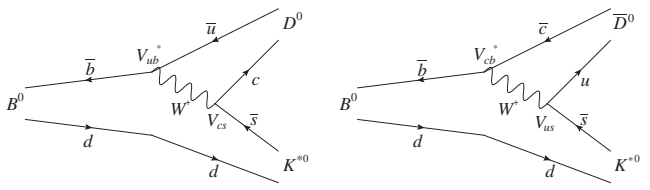

FIG. 1. Feynman diagrams of (left) $B^0 \to D^0K^{*0}$ and (right) $B^0 \to \bar{D}^0K^{*0}$.

[*] Full author list given at the end of the article.

Published by the American Physical Society under the terms of the Creative Commons Attribution 3.0 License. Further distribution of this work must maintain attribution to the author(s) and the published articles title, journal citation, and DOI.

 © 2014 CERN, for the LHCb Collaboration

amplitudes and p is a point in the three-body phase space of the B^0 meson. The integrals are defined over the phase space considered here, namely in a $K^+\pi^-$ mass range of ± 50 MeV$/c^2$ around the nominal K^{*0} mass [10] and for an absolute value of the cosine of the helicity angle θ^* greater than 0.4, where θ^* is defined as the angle between the K momentum and the opposite of the B momentum in the K^{*0} rest frame. The formalism of Eqs. (2)–(4) applies to the generic three-body decay $B^0 \to DK^+\pi^-$ with any number of intermediate resonances included. The integration range is restricted here to the K^{*0} resonance in order to obtain a large value of the coherence factor.

This paper presents two measurements of the ratio, $\mathcal{R}_{CP+}$, of flavor-averaged partial widths of the $B^0 \to D K^{*0}$ decay with the D decaying to a CP-even eigenstate,

$$\mathcal{R}_{CP+} \equiv 2 \times \frac{\Gamma(\bar{B}^0 \to D_{CP+}\bar{K}^{*0}) + \Gamma(B^0 \to D_{CP+}K^{*0})}{\Gamma(\bar{B}^0 \to D^0\bar{K}^{*0}) + \Gamma(B^0 \to \bar{D}^0 K^{*0})}. \tag{5}$$

The relation above is approximated using specific final states of the D meson as $\mathcal{R}_{CP+} \approx \mathcal{R}_d^{hh}$, neglecting corrections from doubly Cabibbo-suppressed $D^0 \to K^+\pi^-$ decays, with

$$\mathcal{R}_d^{hh} \equiv \frac{\Gamma(\bar{B}^0 \to D(h^+h^-)\bar{K}^{*0}) + \Gamma(B^0 \to D(h^+h^-)K^{*0})}{\Gamma(\bar{B}^0 \to D(K^-\pi^+)\bar{K}^{*0}) + \Gamma(B^0 \to D(K^+\pi^-)K^{*0})} \times \frac{\mathcal{B}(D^0 \to K^-\pi^+)}{\mathcal{B}(D^0 \to h^+h^-)}, \tag{6}$$

where h represents either a π or a K meson. This quantity is related to the γ angle and the hadronic parameters by [11]

$$\mathcal{R}_d^{hh} = \frac{1 + r_B^2 + 2r_B\kappa\cos\delta_B\cos\gamma}{1 + r_B^2 r_D^2 + 2r_B r_D\kappa\cos(\delta_B - \delta_D)\cos\gamma}, \tag{7}$$

where r_D and δ_D are the magnitude of the ratio and the phase difference, respectively, between the amplitudes of the $D^0 \to K^+\pi^-$ and $D^0 \to K^-\pi^+$ decays. Charm mixing and CP violation in the decays of D mesons have an effect on the determination of γ [7,12] but are neglected here because of the large expected value of r_B.

Measurements of the $\bar{B}^0$-B^0 partial decay-rate asymmetry, $\mathcal{A}_d^{hh}$, using $D \to h^+h^-$ final states are also presented,

$$\mathcal{A}_d^{hh} \equiv \frac{\Gamma(\bar{B}^0 \to D(h^+h^-)\bar{K}^{*0}) - \Gamma(B^0 \to D(h^+h^-)K^{*0})}{\Gamma(\bar{B}^0 \to D(h^+h^-)\bar{K}^{*0}) + \Gamma(B^0 \to D(h^+h^-)K^{*0})} = \frac{2r_B\kappa\sin\delta_B\sin\gamma}{1 + r_B^2 + 2r_B\kappa\cos\delta_B\cos\gamma}. \tag{8}$$

The $\bar{B}^0$-B^0 asymmetry, $\mathcal{A}_d^{K\pi}$, obtained from the Cabibbo-favored decay $B^0 \to DK^{*0}$ with $D \to K^+\pi^-$, where the two kaons from the D and the K^{*0} decay have the same sign, is

$$\mathcal{A}_d^{K\pi} \equiv \frac{\Gamma(\bar{B}^0 \to D(K^-\pi^+)\bar{K}^{*0}) - \Gamma(B^0 \to D(K^+\pi^-)K^{*0})}{\Gamma(\bar{B}^0 \to D(K^-\pi^+)\bar{K}^{*0}) + \Gamma(B^0 \to D(K^+\pi^-)K^{*0})} = \frac{2r_B r_D\kappa\sin(\delta_B - \delta_D)\sin\gamma}{1 + r_B^2 r_D^2 + 2r_B r_D\kappa\cos(\delta_B - \delta_D)\cos\gamma}. \tag{9}$$

The Cabibbo-suppressed decay $B^0 \to DK^{*0}$ with $D \to \pi^+K^-$, where the two kaons have opposite charge, is studied for the first time by LHCb. The ratios of suppressed $B^0 \to D(\pi^+K^-)K^{*0}$ to favored $B^0 \to D(K^+\pi^-)K^{*0}$ partial widths are measured separately for B^0 and $\bar{B}^0$, and defined as $\mathcal{R}_d^+$ and $\mathcal{R}_d^-$, respectively,

$$\mathcal{R}_d^+ \equiv \frac{\Gamma(B^0 \to D(\pi^+K^-)K^{*0})}{\Gamma(B^0 \to D(K^+\pi^-)K^{*0})} = \frac{r_B^2 + r_D^2 + 2r_B r_D\kappa\cos(\delta_B + \delta_D + \gamma)}{1 + r_B^2 r_D^2 + 2r_B r_D\kappa\cos(\delta_B - \delta_D + \gamma)}, \tag{10}$$

$$\mathcal{R}_d^- \equiv \frac{\Gamma(\bar{B}^0 \to D(\pi^-K^+)\bar{K}^{*0})}{\Gamma(\bar{B}^0 \to D(K^-\pi^+)\bar{K}^{*0})} = \frac{r_B^2 + r_D^2 + 2r_B r_D\kappa\cos(\delta_B + \delta_D - \gamma)}{1 + r_B^2 r_D^2 + 2r_B r_D\kappa\cos(\delta_B - \delta_D - \gamma)}. \tag{11}$$

In pp collisions, B_s^0 mesons are produced and can decay to the same final state, $B_s^0 \to D\bar{K}^{*0}$ [13]. Similar asymmetry observables to those defined above for B^0 mesons are measured with B_s^0 mesons. These are the $\bar{B}_s^0$-B_s^0 asymmetry, $\mathcal{A}_s^{hh}$, obtained from the K^+K^- and $\pi^+\pi^-$ final states of the D meson,

$$\mathcal{A}_s^{hh} \equiv \frac{\Gamma(\bar{B}_s^0 \to D(h^+h^-)K^{*0}) - \Gamma(B_s^0 \to D(h^+h^-)\bar{K}^{*0})}{\Gamma(\bar{B}_s^0 \to D(h^+h^-)K^{*0}) + \Gamma(B_s^0 \to D(h^+h^-)\bar{K}^{*0})}, \tag{12}$$

and the asymmetry, $\mathcal{A}_s^{\pi K}$, from the Cabibbo-favored decay $B_s^0 \to D(\pi^-K^+)\bar{K}^{*0}$, where the two kaons have opposite charge,

$$\mathcal{A}_s^{\pi K} \equiv \frac{\Gamma(\bar{B}_s^0 \to D(\pi^+K^-)K^{*0}) - \Gamma(B_s^0 \to D(\pi^-K^+)\bar{K}^{*0})}{\Gamma(\bar{B}_s^0 \to D(\pi^+K^-)K^{*0}) + \Gamma(B_s^0 \to D(\pi^-K^+)\bar{K}^{*0})}. \tag{13}$$

The $B_s^0 \to D(K^-\pi^+)\bar{K}^{*0}$ decay, where the two kaons have the same charge, is highly suppressed and therefore

unobserved with the current data sample. Finally, the ratios of the flavor-averaged partial widths of the B^0 and B_s^0 decays, when the D meson is reconstructed as $D \to h^+h^-$, $\mathcal{R}_{ds}^{hh}$, are also considered,

$$\mathcal{R}_{ds}^{hh} \equiv \frac{\Gamma(\bar{B}^0 \to D(h^+h^-)\bar{K}^{*0}) + \Gamma(B^0 \to D(h^+h^-)K^{*0})}{\Gamma(\bar{B}_s^0 \to D(h^+h^-)K^{*0}) + \Gamma(B_s^0 \to D(h^+h^-)\bar{K}^{*0})}. \tag{14}$$

The observables related to B_s^0 decays could in principle also be used to determine the value of γ. However, the observables pertaining to B^0 mesons are far more sensitive, owing to the fact that the ratio of interfering amplitudes is closer to unity. Those related to B_s^0 mesons are measured and reported in this paper but are not yet precise enough to provide any constraint on γ.

II. THE LHCb DETECTOR, DATA SET AND EVENT SELECTION

The study reported here is based on a data sample of pp collisions obtained from 3.0 fb^{-1} of integrated luminosity with the LHCb detector [14]. The center-of-mass energy was 7 TeV during the year 2011, when approximately 1/3 of the data were collected, and 8 TeV during the year 2012.

The LHCb detector [14] is a single-arm forward spectrometer covering the pseudorapidity range $2 < \eta < 5$, designed for the study of particles containing b or c quarks. The detector includes a high-precision tracking system consisting of a silicon-strip vertex detector surrounding the pp interaction region [15], a large-area silicon-strip detector located upstream of a dipole magnet with a bending power of about 4 Tm, and three stations of silicon-strip detectors and straw drift tubes placed downstream of the magnet. The tracking system provides a measurement of momentum, p, with a relative uncertainty that varies from 0.4% at low momentum to 0.6% at 100 GeV/c. The minimum distance of a track to a primary vertex, the impact parameter, is measured with a resolution of $(15 + 29/p_{\mathrm{T}})$ μm, where p_{T} is the component of p transverse to the beam, in GeV/c. Different types of charged hadrons are distinguished using information from two ring-imaging Cherenkov detectors [16]. Photon, electron and hadron candidates are identified by a calorimeter system consisting of scintillating-pad and preshower detectors, an electromagnetic calorimeter and a hadronic calorimeter. Muons are identified by a system composed of alternating layers of iron and multiwire proportional chambers. The trigger [17] consists of a hardware stage, based on information from the calorimeter and muon systems, followed by a software stage, which applies a full event reconstruction.

The analysis uses events triggered at the hardware level either when one of the charged tracks of the signal decay gives a large enough energy deposit in the calorimeter system (hadron trigger) or when one of the particles in the event, not reconstructed as forming the signal candidate, fulfills any trigger requirement (i.e. mainly events triggered by one high p_{T} muon, hadron, photon or electron coming from the decay of the other B meson in the event). The software trigger requires a two-, three- or four-track secondary vertex with a large sum of the p_{T} of the charged particles and a significant displacement from the primary pp interaction vertices (PVs). At least one charged particle should have $p_{\mathrm{T}} > 1.7$ GeV/c and χ^2_{IP} with respect to any PV greater than 16, where χ^2_{IP} is defined as the difference in χ^2 of a given PV reconstructed with and without the considered particle. A multivariate algorithm [18] is used for the identification of secondary vertices consistent with the decay of a b hadron.

Approximately 1 million simulated events are used to describe the signal shapes and to compute the efficiencies when data-driven methods are not available. In the simulation, pp collisions are generated using PYTHIA [19,20] with a specific LHCb configuration [21]. Decays of hadronic particles are described by EvtGen [22], in which final state radiation is generated using PHOTOS [23]. The interaction of the generated particles with the detector and its response are implemented using the GEANT4 toolkit [24] as described in Ref. [25].

Candidate $B^0 \to DK^{*0}$ decays are reconstructed in events fulfilling these trigger conditions combining D mesons reconstructed in the $K^{\pm}\pi^{\mp}$, K^+K^- and $\pi^+\pi^-$ decays and K^{*0} mesons reconstructed in the $K^+\pi^-$ final state. The invariant masses of the D and K^{*0} mesons are required to be within 20 MeV/c^2 and 50 MeV/c^2 of their known masses [10], respectively. The B candidate momentum is refit constraining the mass of the D meson to its known value. It is required that $|\cos\theta^*| > 0.4$.

A boosted decision tree (BDT) [26] is used with the algorithm described in Ref. [27] to separate signal from combinatorial background. Separate BDTs are optimized for $K^{\pm}\pi^{\mp}$, K^+K^- and $\pi^+\pi^-$ final states of the D meson. In all cases the samples used to train the BDT are fully simulated events for the signal and candidates from the upper sideband of the B mass distribution in data for the background. This upper sideband is defined as events with a DK^{*0} invariant mass between 5.8 GeV/c^2 and 7 GeV/c^2, lying outside the region used for the fit described in Sec. III. The variables used by the BDT to differentiate signal and background are the following: the p_{T} of each particle in the final state; the fit quality of the D and B^0 vertices; the K^{*0}, D and B^0 χ^2_{IP}; the angle between the B^0 momentum and the vector from the PV to the B^0 decay vertex; the significance of the displacement of the four final-state tracks from the PV.

Thresholds on the BDT classifier are optimized with respect to the signal significance of the B^0 decay modes for the three final states $B^0 \to D(\pi^+K^-)K^{*0}$, $B^0 \to D(K^+K^-)K^{*0}$ and $B^0 \to D(\pi^+\pi^-)K^{*0}$, where the significance is defined as $S/\sqrt{S+B}$ with S and B the

expected number of signal and background candidates. The efficiencies of the selection based on the BDT output classifier are equal to 69%, 71% and 75% for the $D \to K^{\pm}\pi^{\mp}$, $D \to K^{+}K^{-}$ and $D \to \pi^{+}\pi^{-}$ decay channels, respectively.

To improve the purity of the data sample, further selection requirements are made in addition to the BDT. Particle identification (PID) criteria are applied and only well identified pions and kaons are retained. The kaon identification efficiency of the PID criteria is equal to 87% with a pion misidentification rate of 5%. Possible contamination from $\Lambda_b^0 \to \bar{D}^0 p h^-$ decays is reduced by keeping only kaon candidates incompatible with being a proton.

A potentially significant background is due to events where the K from $D \to K^{\pm}\pi^{\mp}$ decays is misidentified as a π and the π is simultaneously misidentified as a K. This causes cross feed from the favored $B^0 \to D(K^+\pi^-)K^{*0}$ decay into the suppressed $B^0 \to D(\pi^+K^-)K^{*0}$ decay. A veto is applied on the D invariant mass computed with a pion mass assignment for the kaon and a kaon mass assignment for the pion. Only candidates for which this invariant mass differs by more than 7 MeV/c^2 from the known D^0 mass [10] are kept, reducing this background to a negligible level while keeping 97% of the signal candidates.

Another potential background is due to charmless decays $B^0 \to h^{\pm}h'^{\mp}K^+\pi^-$, where h' is also π or K. It is removed by requiring the D flight distance with respect to the B vertex to exceed 3 times its uncertainty. Specific peaking backgrounds from $B^0_{(s)} \to D^{\mp}_{(s)}h^{\pm}$ decays are eliminated by applying a veto on candidates for which the invariant mass of three of the four charged mesons is compatible within ± 15 MeV/c^2 of the known D^+ or D_s^+ masses.

After all selections are applied, 0.9% of the events contain more than one signal candidate. Only the candidate with the largest B flight distance with respect to the PV, divided by its uncertainty, is retained. In case several PVs are reconstructed, the PV with respect to which the B candidate has the smallest displacement is used.

Figure 2 shows the background-subtracted $K^+\pi^-$ invariant mass of the K^{*0} candidates used to reconstruct $B^0 \to D(K^+\pi^-)K^{*0}$ decays, obtained with the *sPlot* technique [28]. All selections described above have been applied except the requirement on the K^{*0} candidate mass. This distribution is fitted with a relativistic Breit-Wigner function to describe the K^{*0} signal and a first-order polynomial for the non-K^{*0} contribution. From the fit result, it is estimated that $(8.4 \pm 3.4)\%$ of the signal B^0 candidates are formed with a $K^+\pi^-$ pair that does not originate from a K^{*0} decay, in the $K^+\pi^-$ mass region considered for the analysis.

III. INVARIANT MASS FIT

The numbers of reconstructed signal B^0 and B_s^0 candidates are determined from an unbinned maximum-likelihood fit to the DK^{*0} invariant mass distributions. Candidates are split into eight categories, which are fitted simultaneously: $D(K^+\pi^-)K^{*0}$, $D(K^-\pi^+)\bar{K}^{*0}$, $D(\pi^+K^-)K^{*0}$, $D(\pi^-K^+)\bar{K}^{*0}$, $D(K^+K^-)K^{*0}$, $D(K^+K^-)\bar{K}^{*0}$, $D(\pi^+\pi^-)K^{*0}$ and $D(\pi^+\pi^-)\bar{K}^{*0}$ candidates. The mass distribution of each category is fitted with a sum of probability density functions (PDFs) modeling the various contributing components:

(1) The B^0 and B_s^0 signals are both described by a sum of two Gaussian functions with a common mean.
(2) The combinatorial background is described by an exponential function.
(3) The cross feed from $B^0 \to D\rho^0$ decays, where one π from the $\rho^0 \to \pi^+\pi^-$ decay is misidentified as a K, is described by a nonparametric PDF [29] determined from simulation.
(4) The partially reconstructed $B^0 \to D^*K^{*0}$ and $\bar{B}_s^0 \to D^*K^{*0}$ decays, where D^* stands for D^{*0} or $\bar{D}^{*0}$ with the π^0 or γ from the $D^{*0} \to D^0\pi^0$ or $D^{*0} \to D^0\gamma$ decay not reconstructed, are each modeled by nonparametric PDFs determined from simulation.

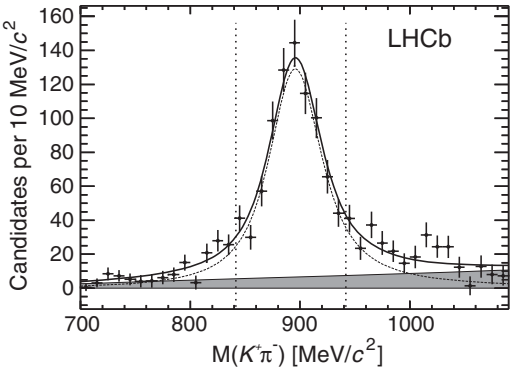

FIG. 2. Background-subtracted $K^{*0} \to K^+\pi^-$ invariant mass for $B^0 \to D(K^+\pi^-)K^{*0}$ signal candidates. The data (points) and the fit described in the text (solid line) are shown. The dashed line represents the K^{*0} signal and the filled area the non-K^{*0} contribution to the $B^0 \to DK^{*0}$ signal. The vertical dotted lines indicate the invariant mass region used in the analysis.

A separate fit to $B^0 \to D(K^+\pi^-)\rho^0$ candidates in the same data sample is performed, reconstructing ρ^0 in the $\pi^+\pi^-$ final state within a ± 50 MeV/c^2 mass range around the known ρ^0 mass. The observed number of $B^0 \to D(K^+\pi^-)\rho^0$ candidates is used, along with the efficiency to reconstruct $B^0 \to D(K^+\pi^-)\rho^0$ candidates as $B^0 \to D(K^+\pi^-)K^{*0}$ from simulation, to constrain the number of cross-feed events in the $D(K^+\pi^-)K^{*0}$ category. The numbers of cross-feed candidates in the other categories are derived from the $D(K^+\pi^-)K^{*0}$ category using the relative D branching fractions from Ref. [10] and selection efficiencies from simulation. As a negligible CP asymmetry is expected for the $B^0 \to D(K^+\pi^-)\rho^0$ background, the numbers of cross-feed events in the $D\bar{K}^{*0}$ categories are constrained to be identical to those of the corresponding DK^{*0} categories.

The partially reconstructed background accumulates at masses lower than the known B^0 mass. Its shape depends on the unknown fraction of longitudinal polarization in the $B^0 \to D^* K^{*0}$ and $\bar{B}^0_s \to D^* K^{*0}$ decays, i.e. the probability that the D^* in these decays is produced with helicity equal to 0. In order to model the $\bar{B}^0_s \to D^* K^{*0}$ contribution, a PDF is built from a linear combination of two nonparametric functions corresponding to the three orthogonal helicity amplitudes. Two of the orthogonal helicity amplitudes result in the same distribution in invariant mass because of parity conservation in the $D^{*0} \to D^0\gamma$ decay, hence simplifying the model. Each function, modeled from simulated events, corresponds to the weighted sum of the $D^{*0} \to D^0\gamma$ and $D^{*0} \to D^0\pi^0$ contributions for a defined helicity eigenstate, where the weights take into account the relative D^{*0} decay branching fractions from Ref. [10] and the corresponding efficiencies from simulation. The $B^0 \to D^* K^{*0}$ background is modeled in a similar way, shifting the shape obtained for the $\bar{B}^0_s \to D^* K^{*0}$ decay by the known difference between the B^0 and B^0_s masses [10]. The coefficients of the two functions in the linear combinations are different for the $B^0 \to D^* K^{*0}$ and $\bar{B}^0_s \to D^* K^{*0}$ decays but are common to the eight categories and are free parameters in the fit.

The yields of the B^0_s and $\bar{B}^0_s$ partially reconstructed backgrounds in the $D(K^+\pi^-)K^{*0}$ categories are fixed to zero since the $\bar{B}^0_s \to D^* K^{*0}$ decay modes have negligible total branching fractions when the kaons from the D and K^{*0} have the same charge sign. The yields of the $B^0_s \to D^* \bar{K}^{*0}$ and $\bar{B}^0_s \to D^* K^{*0}$ backgrounds in the $D(\pi^+K^-)K^{*0}$ categories are constrained to be the same because *CP* violation is expected to be negligible for this background. Additional constraints on the normalizations of the $\bar{B}^0_s \to D^* K^{*0}$ backgrounds in the $D(K^+K^-)K^{*0}$ and $D(\pi^+\pi^-)K^{*0}$ categories, relative to the $D(\pi^+K^-)K^{*0}$ categories, are imposed using the relevant D decay branching fractions from Ref. [10] and selection efficiencies obtained from simulation.

There are 35 free parameters in the fit: the B^0 peak position; the core Gaussian resolution for the B^0 and the B^0_s signal shapes; the slope of the combinatorial background, which is different for each D meson final state (one parameter for $D \to K^\pm\pi^\mp$, one for $D \to K^+K^-$ and one for $D \to \pi^+\pi^-$); the fractions of longitudinal polarization in

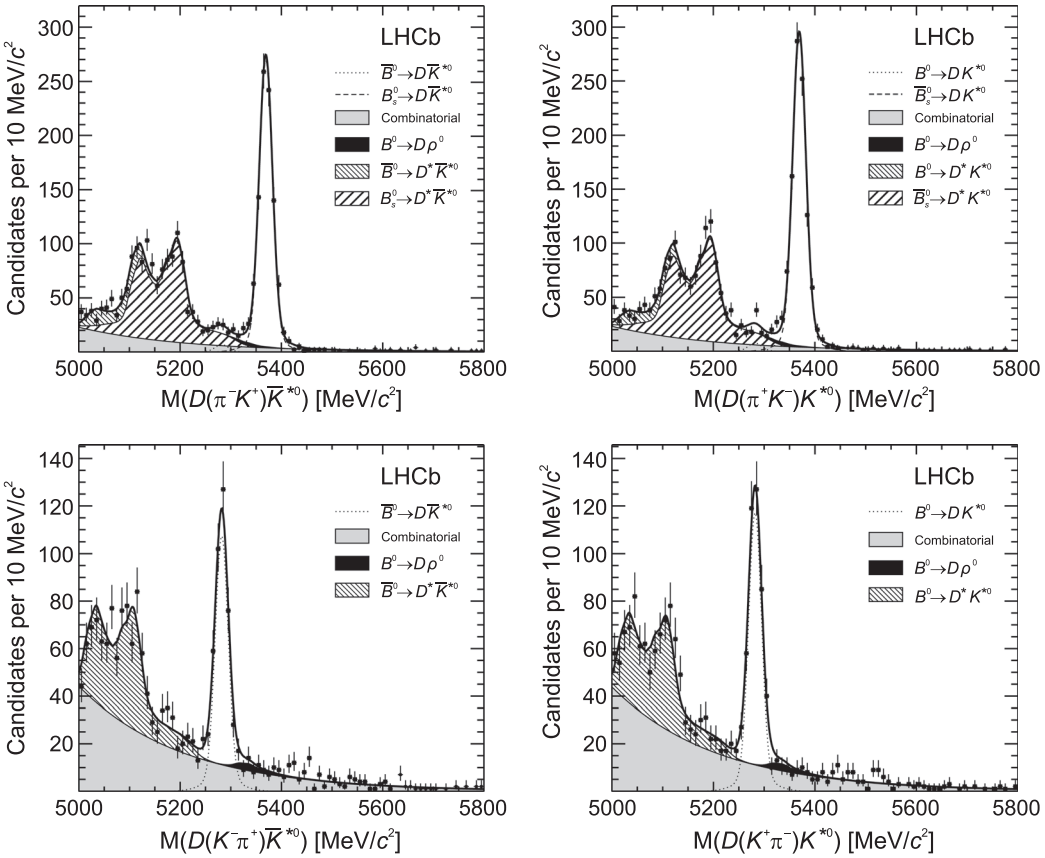

FIG. 3. Distributions of (top left) $D(\pi^-K^+)\bar{K}^{*0}$, (top right) $D(\pi^+K^-)K^{*0}$, (bottom left) $D(K^-\pi^+)\bar{K}^{*0}$ and (bottom right) $D(K^+\pi^-)K^{*0}$ invariant mass. The data (black points) and the fitted invariant mass model (thick solid line) are shown. The PDFs corresponding to the different species are indicated in the legend: the B^0 signal, the B^0_s signal, combinatorial background, $B^0 \to D\rho^0$ background, partially reconstructed $B^0_s \to D^*\bar{K}^{*0}$ and $B^0 \to D^*K^{*0}$ backgrounds.

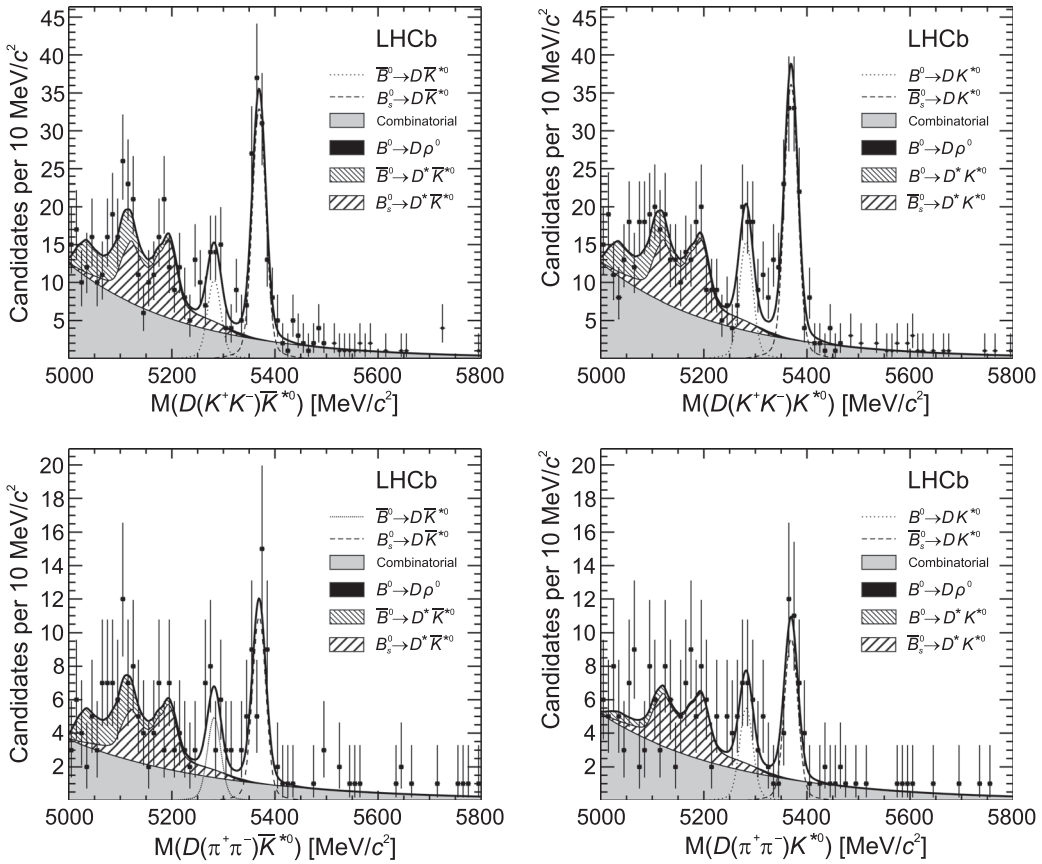

FIG. 4. Distributions of (top left) $D(K^+K^-)\bar{K}^{*0}$, (top right) $D(K^+K^-)K^{*0}$, (bottom left) $D(\pi^+\pi^-)\bar{K}^{*0}$ and (bottom right) $D(\pi^+\pi^-)K^{*0}$ invariant mass. The data (black points) and the fitted invariant mass model (thick solid line) are shown. The PDFs corresponding to the different species are indicated in the legend: the B^0 signal, the B^0_s signal, combinatorial background, $B^0 \to D\rho^0$ background and partially reconstructed $B^0_s \to D^*\bar{K}^{*0}$ and $B^0 \to D^*K^{*0}$ backgrounds.

the $B^0 \to D^*K^{*0}$ and $\bar{B}^0_s \to D^*K^{*0}$ backgrounds and the yields for each fit component within each category. *CP* violation in $B^0 \to D^*K^{*0}$ decays is allowed by floating the yields of this background in the DK^{*0} and $D\bar{K}^{*0}$ categories separately. The difference between the central value of the B^0_s and B^0 mass is fixed to its known value from Ref. [10] and the ratio between the signal Gaussian resolutions is fixed from the simulation.

The nonparametric functions used to model all the specific backgrounds are smeared to take into account the different mass resolutions observed in data and simulation. The invariant mass distributions together with the function resulting from the fit are shown in Figs. 3 and 4. The numbers of signal events in each category are summarized in Table I.

IV. SYSTEMATIC UNCERTAINTIES

The signal yields determined from the invariant mass fit are corrected in order to evaluate the asymmetries and ratios described in Eqs. (5)–(13). These corrections account for selection efficiency and detection asymmetry, $\bar{B}$-B production asymmetry and its dilution due to mixing, misidentification of D meson decays, D^0 decay branching fractions,

TABLE I. Yields of signal candidates with their statistical uncertainties.

Channel	Signal yield	Channel	Signal yield
$\bar{B}^0 \to D(\pi^-K^+)\bar{K}^{*0}$	24 ± 12	$B^0 \to D(\pi^+K^-)K^{*0}$	26 ± 12
$\bar{B}^0 \to D(K^-\pi^+)\bar{K}^{*0}$	370 ± 22	$B^0 \to D(K^+\pi^-)K^{*0}$	405 ± 23
$\bar{B}^0 \to D(K^+K^-)\bar{K}^{*0}$	36 ± 9	$B^0 \to D(K^+K^-)K^{*0}$	53 ± 10
$\bar{B}^0 \to D(\pi^+\pi^-)\bar{K}^{*0}$	18 ± 6	$B^0 \to D(\pi^+\pi^-)K^{*0}$	21 ± 7
$B^0_s \to D(\pi^-K^+)\bar{K}^{*0}$	933 ± 33	$\bar{B}^0_s \to D(\pi^+K^-)K^{*0}$	993 ± 34
$B^0_s \to D(K^+K^-)\bar{K}^{*0}$	115 ± 12	$\bar{B}^0_s \to D(K^+K^-)K^{*0}$	125 ± 13
$B^0_s \to D(\pi^+\pi^-)\bar{K}^{*0}$	39 ± 7	$\bar{B}^0_s \to D(\pi^+\pi^-)K^{*0}$	35 ± 7

TABLE II. Uncertainties in the observables. All model-related systematic uncertainties are added in quadrature and the result is shown as one source of systematic uncertainty. The presence of "—" indicates that the source of uncertainty does not affect the observable.

Source	Observable											
	$\mathcal{A}_d^{KK}$	$\mathcal{A}_d^{\pi\pi}$	$\mathcal{R}_d^{KK}$	$\mathcal{R}_d^{\pi\pi}$	$\mathcal{R}_d^{+}$	$\mathcal{R}_d^{-}$	$\mathcal{R}_{ds}^{KK}$	$\mathcal{R}_{ds}^{\pi\pi}$	$\mathcal{A}_s^{KK}$	$\mathcal{A}_s^{\pi\pi}$	$\mathcal{A}_d^{K\pi}$	$\mathcal{A}_s^{\pi K}$
Trigger efficiency	0.011	0.011	0.015	0.019	—	—	0.000	0.000	0.011	0.011	0.012	0.012
PID efficiency	0.005	0.005	0.010	0.012	—	—	0.000	0.000	0.005	0.005	0.005	0.005
Selection efficiency	0.014	0.014	0.029	0.037	—	—	0.000	0.000	0.015	0.014	0.014	0.014
Lifetime difference	—	—	—	—	—	—	0.002	0.003	—	—	—	—
Prod. asymmetry	0.005	0.005	0.001	0.000	—	—	0.000	0.001	—	—	0.005	—
$D \to K\pi$ misID	—	—	—	—	0.000	0.001	—	—	—	—	—	—
D^0 decay BFs	—	—	0.025	0.028	—	—	—	—	—	—	—	—
f_s/f_d	—	—	—	—	—	—	0.008	0.012	—	—	—	—
τ_s/τ_d	—	—	—	—	—	—	0.001	0.001	—	—	—	—
Model related	0.004	0.001	0.011	0.012	0.010	0.011	0.002	0.001	0.004	0.002	0.001	0.000
Total systematic	0.020	0.019	0.044	0.053	0.010	0.011	0.009	0.012	0.020	0.019	0.020	0.019
Statistical	0.144	0.217	0.159	0.268	0.028	0.031	0.017	0.038	0.073	0.131	0.041	0.025

hadronization fractions and biases introduced by the fit model. The uncertainties in these corrections cause systematic uncertainties in the results. Systematic uncertainties are also introduced by the uncertainties in the various constraints on the invariant mass model. The systematic uncertainties incurred from all sources are obtained combining in quadrature the individual uncertainties and are summarized in Table II.

A. Efficiencies

Separate corrections are applied to account for differing trigger and PID efficiencies. These efficiencies are obtained from real data by means of low-background calibration samples of kaons and pions from $D^{*\pm} \to D(K^{\mp}\pi^{\pm})\pi^{\pm}$ decays [30]. They are evaluated separately for $\bar{B}$ and B modes to account for detection asymmetries. The relative trigger and PID efficiencies differ from unity by 1% and 5%, respectively, and their uncertainties result in the systematic uncertainties given in Table II.

Another correction is applied to account for the differences in the kinematic selection requirements of the different decay modes. The efficiencies are evaluated from simulated data, and they are assumed to be equal for the $B^0 \to D(K^+\pi^-)K^{*0}$ and $B^0 \to D(\pi^+K^-)K^{*0}$ decays. They differ between decay modes by 8% at maximum. The uncertainties on these efficiencies affect the measured observables as shown in Table II. It is noted that the $\mathcal{R}_d^{\pm}$ observables have no systematic uncertainty from selection efficiency. This is because they are separated by B meson flavor and have the same D meson final state; therefore all efficiencies are assumed to cancel.

Because of the different B^0 and B_s^0 lifetimes, the ratio of efficiencies for $B^0 \to D(h^+h'^-)K^{*0}$ to $\bar{B}_s^0 \to D(h'^+h^-)K^{*0}$ is different from one. This ratio is assumed to be equal between all the D meson final states and is calculated using the $B^0 \to D(K^+\pi^-)K^{*0}$ and $\bar{B}_s^0 \to D(\pi^+K^-)K^{*0}$ decay modes, assuming that the lifetime difference effects factorize from the other selection effects. The difference in B^0 and B_s^0 selection efficiencies arises from the use of variables sensitive to the decay topology in the BDT and is equal to 3%. The systematic uncertainty from this source is labeled "Lifetime difference" in Table II. The only observables affected by the systematic uncertainty due to lifetime difference are the $\mathcal{R}_{ds}^{hh}$ observables, since only these involve both B^0 and B_s^0 partial widths.

B. Production asymmetry

The difference between B^0 and $\bar{B}^0$, or B_s^0 and $\bar{B}_s^0$, production rates in pp collisions is accounted for by applying a correction factor $a_P = (1 - \alpha A_P)/(1 + \alpha A_P)$ to the $\bar{B}^0$ and $\bar{B}_s^0$ signal yields, where

$$A_P \equiv \frac{\sigma(\bar{B}) - \sigma(B)}{\sigma(\bar{B}) + \sigma(B)} \tag{15}$$

is the raw production asymmetry of the B^0 or B_s^0 mesons in question. In the case of B^0 mesons, A_P has been measured, using $B^0 \to J/\psi K^{*0}$ decays, to be $A_P = 0.010 \pm 0.013$ [31]. The effect of the raw production asymmetry on the number of observed $\bar{B}^0$ or B^0 decays becomes less pronounced for larger decay times due to mixing. It is also affected by the selection efficiency as a function of the decay time, $\epsilon(B^0 \to DK^{*0}, t)$. A factor, α, accounts for this dilution and is given for B^0 mesons by

$$\alpha = \frac{\int_0^{+\infty} e^{-t/\tau_{B^0}} \cos(\Delta m_d t)\epsilon(B^0 \to DK^{*0}, t)\mathrm{d}t}{\int_0^{+\infty} e^{-t/\tau_{B^0}} \epsilon(B^0 \to DK^{*0}, t)\mathrm{d}t}, \tag{16}$$

where Δm_d is the B^0-$\bar{B}^0$ oscillation frequency and τ_{B^0} is the B^0 lifetime.

The factor α is evaluated separately for each $B^0 \to D(K^{\pm}\pi^{\mp})K^{*0}$, $B^0 \to D(K^+K^-)K^{*0}$ and $B^0 \to D(\pi^+\pi^-)K^{*0}$ decays since it is dependent on the separately optimized

selection requirements. The resulting values of α are 0.362 ± 0.014, 0.391 ± 0.014 and 0.398 ± 0.014, respectively. These figures are computed using fully simulated events and data-driven PID efficiencies from calibration samples. The uncertainty on a_P is propagated to the measured observables to estimate the systematic uncertainty from the production asymmetry and mixing. Owing to the large B_s^0 oscillation frequency, a potential production asymmetry of B_s^0 mesons does not significantly affect the measurements presented here and is neglected.

C. Misidentification of D meson decays

Favored $B^0 \to D(K^+\pi^-)K^{*0}$ decays are misidentified as suppressed $B^0 \to D(\pi^+K^-)K^{*0}$ decays at a small but non-negligible rate. The fraction of signal $B^0 \to D(K^+\pi^-)K^{*0}$ decays reconstructed as signal $B^0 \to D(\pi^+K^-)K^{*0}$ decays is estimated from the simulation to be less than 1% after applying the veto described in Sec. II. However, the best-fit values of the numbers of $B^0 \to D(\pi^+K^-)K^{*0}$ decays are corrected to take this into account. The uncertainty in this correction causes a systematic uncertainty in the $\mathcal{R}_d^{\pm}$ observables given in Table II as misID.

D. Other corrections

Two ratios of D^0 meson decay branching fractions (BF) are needed to compute the final results because of the approximation made between $\mathcal{R}_{CP+}$ and $\mathcal{R}_d^{hh}$ in Eq. (6). These are taken from Ref. [10], the results of which imply that the ratio of $\mathcal{B}(D^0 \to K^-\pi^+)$ to $\mathcal{B}(D^0 \to K^+K^-)$ is 9.80 ± 0.24 and the ratio of $\mathcal{B}(D^0 \to K^-\pi^+)$ to $\mathcal{B}(D^0 \to \pi^+\pi^-)$ is 27.7 ± 0.6.

The fraction of b quarks that hadronize into B^0 and B_s^0 mesons in pp collisions, f_d and f_s, respectively, has an effect on the number of B^0 and B_s^0 mesons produced in LHCb. Since the $\mathcal{R}_{ds}^{hh}$ observables are ratios of B^0 and B_s^0 decay partial widths, they are corrected with the hadronization fraction ratio $f_s/f_d = 0.267 \pm 0.021$ [32]. The $\mathcal{R}_{ds}^{hh}$ observables also contain a factor of $\tau_{B_s^0}/\tau_{B^0}$, which arises because of the lifetimes, τ, of the B^0 and B_s^0 mesons. This is taken from Ref. [10], the results of which imply that $\tau_{B_s^0}/\tau_{B^0} = 0.99 \pm 0.01$.

E. Model-related systematic uncertainty

The B meson invariant mass model is validated with an ensemble of simulated pseudoexperiments. The results of these pseudoexperiments show small biases, of the order of 1% of the statistical uncertainty, in the best-fit values of the signal yields, as determined by the invariant mass fit. The affected signal yields are corrected for these biases before computing the observables. The statistical uncertainty on the bias due to the limited number of pseudoexperiments causes systematic uncertainty in the observables.

Systematic uncertainties due to the effects of the constraints made when constructing the invariant mass fit model are also evaluated with pseudoexperiments. The constraints considered are

(1) The values fixed from simulation of the core fraction and the ratio between the widths of the two Gaussian functions used as signal PDF;
(2) The difference in mass of the B^0 and B_s^0 mesons from Ref. [10];
(3) The branching ratios from Ref. [10] and selection efficiencies from simulation used to constrain the relative normalizations of the background PDFs.

Each fixed parameter of the model has an associated uncertainty. To evaluate this, the invariant mass model is altered such that a particular fixed parameter is varied by its uncertainty and data sets generated with the default model are fitted with this altered value. The variations in the best-fit values of the signal yields observed when changing the model are used to assign a systematic uncertainty on the signal yields. This process is repeated for each fixed parameter and the systematic uncertainties in the signal yields are propagated to the observables. All model-related systematic uncertainties are added in quadrature, and this figure is given in Table II.

V. RESULTS

The results are

$$\begin{aligned}
\mathcal{A}_d^{KK} &= -0.20 \pm 0.15 \pm 0.02, \\
\mathcal{A}_d^{\pi\pi} &= -0.09 \pm 0.22 \pm 0.02, \\
\mathcal{R}_d^{KK} &= 1.05^{+0.17}_{-0.15} \pm 0.04, \\
\mathcal{R}_d^{\pi\pi} &= 1.21^{+0.28}_{-0.25} \pm 0.05, \\
\mathcal{R}_d^{+} &= 0.06 \pm 0.03 \pm 0.01, \\
\mathcal{R}_d^{-} &= 0.06 \pm 0.03 \pm 0.01, \\
\mathcal{R}_{ds}^{KK} &= 0.10 \pm 0.02 \pm 0.01, \\
\mathcal{R}_{ds}^{\pi\pi} &= 0.15 \pm 0.04 \pm 0.01, \\
\mathcal{A}_s^{KK} &= -0.04 \pm 0.07 \pm 0.02, \\
\mathcal{A}_s^{\pi\pi} &= 0.06 \pm 0.13 \pm 0.02, \\
\mathcal{A}_d^{K\pi} &= -0.03 \pm 0.04 \pm 0.02, \\
\mathcal{A}_s^{\pi K} &= -0.01 \pm 0.03 \pm 0.02,
\end{aligned}$$

where the first uncertainties are statistical and the second systematic [33]. The significances of the combined B^0 and $\bar{B}^0$ signals for the $B^0 \to D(\pi^+K^-)K^{*0}$, $B^0 \to D(K^+K^-)K^{*0}$ and $B^0 \to D(\pi^+\pi^-)K^{*0}$ decay modes are 2.9σ, 8.6σ and 5.8σ, respectively, including systematic uncertainties. The statistical significances, expressed in terms of the number of standard deviations (σ), are computed from $\sqrt{2\ln(L_{\rm sig}/L_0)}$ where $L_{\rm sig}$ and L_0 are the likelihoods from the nominal mass fit described in Sec. III and from the same fit omitting the signal component, respectively. The

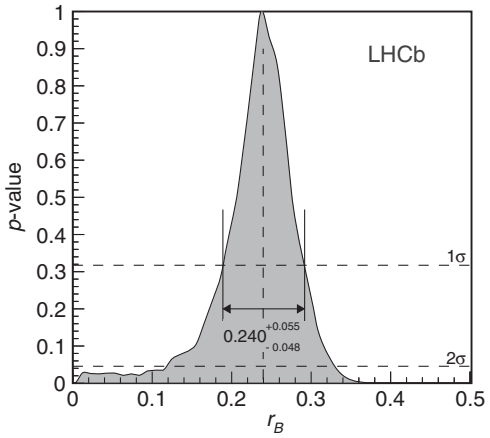

FIG. 5. The p value as a function of r_B, for $\kappa = 0.95 \pm 0.03$. The horizontal dashed lines represent the 1σ and 2σ confidence levels and the vertical dotted line represents the obtained central value.

likelihoods are convolved with a Gaussian function of width equal to the systematic uncertainties on the fit model in order to compute the total significances. No significant *CP* violation effect is observed.

The constraints from the measurements pertaining to B^0 mesons on the angle γ of the unitarity triangle and the hadronic parameters r_B and δ_B are presented in Sec. VI. With more data, improved measurements of the quantities related to $B_s^0 \to D\bar{K}^{*0}$ decays will also contribute to the sensitivity but are not used here.

VI. IMPLICATION ON THE VALUE OF r_B

The sensitivity of these results to the CKM phase γ is investigated by employing a frequentist method described in Ref. [2] to scan the (γ, r_B, δ_B) parameter space and calculate the χ^2 probability at each point, given the measurements of the observables and using Eqs. (7)–(11). The statistical and systematic uncertainties are combined in quadrature and their correlations are accounted for. In principle, the coherence factor κ can also be extracted together with γ, r_B and δ_B, but the uncertainties of the measurements are too large with the current data sample size to constrain all parameters together. A value of $\kappa = 0.95 \pm 0.03$ is used instead. This value is determined from a toy simulation study of a realistic model for the resonance content of $B^0 \to DK^+\pi^-$ decays, similar to the method used in Ref. [34]. This model describes the decay amplitude in the analysis phase space as a superposition of a nonresonant component and amplitudes corresponding to the intermediate $K^*(892)^0$, $K^*(1410)^0$, $K_0^*(1430)^0$, $K_2^*(1430)^0$, $K^*(1680)^0$, $D_0^*(2410)^-$, $D_2^*(2460)^-$ and $D_{s2}(2573)^+$ resonances. The relative fractions and phases between these components are generated randomly according to their known values and uncertainties [10] when they have been observed or within conservatively large ranges when they have not been measured. The analysis selection effects are taken into account, and the main requirements affecting the value of κ are the $K^*(892)^0$ mass selection of 50 MeV$/c^2$ around the known mass and the selection on $|\cos\theta^*|$ being larger than 0.4. The $D^0 \to K^\pm\pi^\mp$ amplitude ratio r_D and strong phase difference δ_D are taken from the Heavy Flavor Averaging Group [35].

A one-dimensional projection of the p value, or $1 - \mathrm{CL}$, is given in Fig. 5, which shows that r_B is

$$r_B = 0.240^{+0.055}_{-0.048}$$

at a confidence level of 68.3% and is different from 0 with a significance of 2.7σ. The p value at each point of r_B is computed with simulated pseudoexperiments following a Feldman-Cousins method, where the nuisance parameters are kept at their best-fit values obtained at each point of r_B.

Two-dimensional projections of the p value from the profile likelihood are shown in Fig. 6. The LHCb average value for γ, extracted from a combination of $B^\pm \to DK^\pm$ and $B^\pm \to D\pi^\pm$ analyses [2], is shown with its 68.3% confidence level interval. The precision of the current

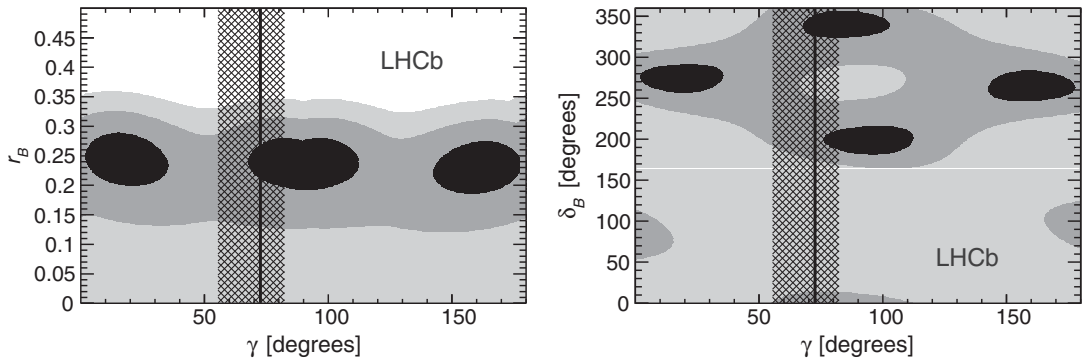

FIG. 6. Two-dimensional projections of the p value in (r_B, δ_B, γ) parameter space onto (left) r_B and γ and (right) δ_B and γ, for $\kappa = 0.95 \pm 0.03$. The contours are the $n\sigma$ profile likelihood contours, where $\Delta\chi^2 = n^2$ with $n = 1$ (black), 2 (medium grey) and 3 (light gray), corresponding to 39.4%, 86.5% and 98.9% confidence level, respectively. The vertical line and hashed band represent the best-fit value of γ and the 68.3% confidence level interval by Ref. [2].

results does not allow a significant measurement of γ from $B^0 \to DK^{*0}$ decays alone, but these measurements could nonetheless be used in a global fit.

VII. CONCLUSIONS

The parameters of the $B^0 \to DK^{*0}$ decay, which are sensitive to the CKM angle γ, have been measured with a sample of 3.0 fb^{-1} of LHC pp collision data collected by the LHCb detector. The results include the first measurements of CP asymmetries in B^0 and $\bar{B}^0_s$ to DK^{*0} decays with the neutral D meson decaying into the $\pi^+\pi^-$ final state. The results related to the K^+K^- final state of the D meson, $\mathcal{A}_d^{KK}$ and $\mathcal{R}_d^{KK}$, are in agreement with and more precise than those from a previous analysis of LHCb data [36], and supersede them. The measurements of $\mathcal{R}_d^+$ and $\mathcal{R}_d^-$ presented here are the first obtained separately for B^0 and $\bar{B}^0$ mesons. They are consistent with the measurement of the flavor-averaged ratio

$$\frac{\Gamma(\bar{B}^0 \to D(\pi^-K^+)\bar{K}^{*0}) + \Gamma(B^0 \to D(\pi^+K^-)K^{*0})}{\Gamma(\bar{B}^0 \to D(K^-\pi^+)\bar{K}^{*0}) + \Gamma(B^0 \to D(K^+\pi^-)K^{*0})} \quad (17)$$

by the Belle Collaboration [37] using the same K^{*0} invariant mass range.

From the measurements presented in this article, we measure the value of $r_B(DK^{*0})$, the ratio of the amplitudes of the decay $B^0 \to DK^+\pi^-$ with a $b \to u$ or a $b \to c$ transition, in a $K\pi$ mass region of ± 50 MeV$/c^2$ around the $K^*(892)^0$ mass, and for an absolute value of the cosine of the K^{*0} helicity angle larger than 0.4. It is found to be equal to $0.240^{+0.055}_{-0.048}$ at a confidence level of 68.3%. This is the first measurement of this parameter with LHCb data and is more accurate than the previous measurement made by the *BABAR* Collaboration [38], in a comparable region of phase space.

ACKNOWLEDGMENTS

We express our gratitude to our colleagues in the CERN accelerator departments for the excellent performance of the LHC. We thank the technical and administrative staff at the LHCb institutes. We acknowledge support from CERN and from the national agencies: CAPES, CNPq, FAPERJ and FINEP (Brazil); NSFC (China); CNRS/IN2P3 (France); BMBF, DFG, HGF and MPG (Germany); SFI (Ireland); INFN (Italy); FOM and NWO (The Netherlands); MNiSW and NCN (Poland); MEN/IFA (Romania); MinES and FANO (Russia); MinECo (Spain); SNSF and SER (Switzerland); NASU (Ukraine); STFC (United Kingdom); NSF (USA). The Tier1 computing centers are supported by IN2P3 (France), KIT and BMBF (Germany), INFN (Italy), NWO and SURF (The Netherlands), PIC (Spain), GridPP (United Kingdom). We are indebted to the communities behind the multiple open source software packages on which we depend. We are also thankful for the computing resources and the access to software R&D tools provided by Yandex LLC (Russia). Individual groups or members have received support from EPLANET, Marie Skłodowska-Curie Actions and ERC (European Union), Conseil général de Haute-Savoie, Labex ENIGMASS and OCEVU, Région Auvergne (France), RFBR (Russia), XuntaGal and GENCAT (Spain), Royal Society and Royal Commission for the Exhibition of 1851 (United Kingdom).

[1] N. Cabibbo, Phys. Rev. Lett. **10**, 531 (1963); M. Kobayashi and T. Maskawa, Prog. Theor. Phys. **49**, 652 (1973).
[2] R. Aaij *et al.* (LHCb Collaboration), Phys. Lett. B **726**, 151 (2013).
[3] J.-P. Lees *et al.* (*BABAR* Collaboration), Phys. Rev. D **87**, 052015 (2013).
[4] K. Trabelsi (Belle Collaboration), arXiv:1301.2033.
[5] J. Brod and J. Zupan, J. High Energy Phys. 01 (2014) 051.
[6] M. Gronau and D. Wyler, Phys. Lett. B **265**, 172 (1991); M. Gronau and D. London, Phys. Lett. B **253**, 483 (1991); D. Atwood, I. Dunietz, and A. Soni, Phys. Rev. Lett. **78**, 3257 (1997).
[7] D. Atwood, I. Dunietz, and A. Soni, Phys. Rev. D **63**, 036005 (2001).
[8] I. Dunietz, Phys. Lett. B **270**, 75 (1991).
[9] M. Gronau, Phys. Lett. B **557**, 198 (2003).
[10] J. Beringer *et al.* (Particle Data Group), Phys. Rev. D **86**, 010001 (2012), and 2013 partial update for the 2014 edition.
[11] P. del Amo Sanchez *et al.* (*BABAR* Collaboration), Phys. Rev. D **82**, 072004 (2010).
[12] M. Rama, Phys. Rev. D **89**, 014021 (2014).
[13] R. Aaij *et al.* (LHCb Collaboration), Phys. Lett. B **706**, 32 (2011).
[14] A. A. Alves, Jr. *et al.* (LHCb Collaboration), JINST **3**, S08005 (2008).
[15] R. Aaij *et al.*, JINST **9**, P09007 (2014).
[16] M. Adinolfi *et al.*, Eur. Phys. J. C **73**, 2431 (2013).
[17] R. Aaij *et al.*, JINST **8**, P04022 (2013)
[18] V. V. Gligorov and M. Williams, JINST **8**, P02013 (2013).
[19] T. Sjöstrand, S. Mrenna, and P. Skands, J. High Energy Phys. 05 (2006) 026.
[20] T. Sjöstrand, S. Mrenna, and P. Skands, Comput. Phys. Commun. **178**, 852 (2008).
[21] I. Belyaev *et al.*, Nuclear Science Symposium Conference Record (NSS/MIC) 1155 (2010).
[22] D. J. Lange, Nucl. Instrum. Methods Phys. Res., Sect. A **462**, 152 (2001).

[23] P. Golonka and Z. Was, Eur. Phys. J. C **45**, 97 (2006).
[24] J. Allison *et al.* (Geant4 Collaboration), IEEE Trans. Nucl. Sci. **53**, 270 (2006); S. Agostinelli *et al.* (Geant4 Collaboration), Nucl. Instrum. Methods Phys. Res., Sect. A **506**, 250 (2003).
[25] M. Clemencic, G. Corti, S. Easo, C. R. Jones, S. Miglioranzi, M. Pappagallo, and P. Robbe, J. Phys. Conf. Ser. **331**, 032023 (2011).
[26] L. Breiman, J. H. Friedman, R. A. Olshen, and C. J. Stone, *Classification and Regression Trees* (Wadsworth International Group, Belmont, CA, 1984).
[27] R. E. Schapire and Y. Freund, J. Comput. Syst. Sci. **55**, 119 (1997).
[28] M. Pivk and F. R. Le Diberder, Nucl. Instrum. Methods Phys. Res., Sect. A **555**, 356 (2005).
[29] K. S. Cranmer, Comput. Phys. Commun. **136**, 198 (2001).
[30] A. Martín Sánchez, P. Robbe, and M.-H. Schune, Report No. LHCb-PUB-2011-026.
[31] R. Aaij *et al.* (LHCb Collaboration), Phys. Rev. Lett. **108**, 201601 (2012).
[32] R. Aaij *et al.* (LHCb Collaboration), Phys. Rev. D **85**, 032008 (2012).
[33] See Supplemental Material http://link.aps.org/supplemental/10.1103/PhysRevD.90.112002 for the correlation coefficients between the measured values.
[34] S. Pruvot, M.-H. Schune, V. Sordini, and A. Stocchi, arXiv:hep-ph/0703292.
[35] Y. Amhis *et al.* (Heavy Flavor Averaging Group), arXiv:1207.1158, updated results and plots available at http://www.slac.stanford.edu/xorg/hfag/, June 2014, "allowing all CP violation" result.
[36] R. Aaij *et al.* (LHCb Collaboration), J. High Energy Phys. 03 (2013) 067.
[37] K. Negishi *et al.* (Belle Collaboration), Phys. Rev. D **86**, 011101 (2012).
[38] B. Aubert *et al.* (*BABAR* Collaboration), Phys. Rev. D **80**, 031102 (2009).

R. Aaij,[41] B. Adeva,[37] M. Adinolfi,[46] A. Affolder,[52] Z. Ajaltouni,[5] S. Akar,[6] J. Albrecht,[9] F. Alessio,[38] M. Alexander,[51] S. Ali,[41] G. Alkhazov,[30] P. Alvarez Cartelle,[37] A. A. Alves Jr.,[25,38] S. Amato,[2] S. Amerio,[22] Y. Amhis,[7] L. An,[3] L. Anderlini,[17,a] J. Anderson,[40] R. Andreassen,[57] M. Andreotti,[16,b] J. E. Andrews,[58] R. B. Appleby,[54] O. Aquines Gutierrez,[10] F. Archilli,[38] A. Artamonov,[35] M. Artuso,[59] E. Aslanides,[6] G. Auriemma,[25,c] M. Baalouch,[5] S. Bachmann,[11] J. J. Back,[48] A. Badalov,[36] V. Balagura,[31] W. Baldini,[16] R. J. Barlow,[54] C. Barschel,[38] S. Barsuk,[7] W. Barter,[47] V. Batozskaya,[28] V. Battista,[39] A. Bay,[39] L. Beaucourt,[4] J. Beddow,[51] F. Bedeschi,[23] I. Bediaga,[1] S. Belogurov,[31] K. Belous,[35] I. Belyaev,[31] E. Ben-Haim,[8] G. Bencivenni,[18] S. Benson,[38] J. Benton,[46] A. Berezhnoy,[32] R. Bernet,[40] M.-O. Bettler,[47] M. van Beuzekom,[41] A. Bien,[11] S. Bifani,[45] T. Bird,[54] A. Bizzeti,[17,d] P. M. Bjørnstad,[54] T. Blake,[48] F. Blanc,[39] J. Blouw,[10] S. Blusk,[59] V. Bocci,[25] A. Bondar,[34] N. Bondar,[30,38] W. Bonivento,[15,38] S. Borghi,[54] A. Borgia,[59] M. Borsato,[7] T. J. V. Bowcock,[52] E. Bowen,[40] C. Bozzi,[16] T. Brambach,[9] J. van den Brand,[42] J. Bressieux,[39] D. Brett,[54] M. Britsch,[10] T. Britton,[59] J. Brodzicka,[54] N. H. Brook,[46] H. Brown,[52] A. Bursche,[40] G. Busetto,[22,e] J. Buytaert,[38] S. Cadeddu,[15] R. Calabrese,[16,b] M. Calvi,[20,f] M. Calvo Gomez,[36,g] P. Campana,[18,38] D. Campora Perez,[38] A. Carbone,[14,h] G. Carboni,[24,i] R. Cardinale,[19,38,j] A. Cardini,[15] L. Carson,[50] K. Carvalho Akiba,[2] G. Casse,[52] L. Cassina,[20] L. Castillo Garcia,[38] M. Cattaneo,[38] Ch. Cauet,[9] R. Cenci,[58] M. Charles,[8] Ph. Charpentier,[38] S. Chen,[54] S.-F. Cheung,[55] N. Chiapolini,[40] M. Chrzaszcz,[40,26] K. Ciba,[38] X. Cid Vidal,[38] G. Ciezarek,[53] P. E. L. Clarke,[50] M. Clemencic,[38] H. V. Cliff,[47] J. Closier,[38] V. Coco,[38] J. Cogan,[6] E. Cogneras,[5] P. Collins,[38] A. Comerma-Montells,[11] A. Contu,[15] A. Cook,[46] M. Coombes,[46] S. Coquereau,[8] G. Corti,[38] M. Corvo,[16,b] I. Counts,[56] B. Couturier,[38] G. A. Cowan,[50] D. C. Craik,[48] M. Cruz Torres,[60] S. Cunliffe,[53] R. Currie,[50] C. D'Ambrosio,[38] J. Dalseno,[46] P. David,[8] P. N. Y. David,[41] A. Davis,[57] K. De Bruyn,[41] S. De Capua,[54] M. De Cian,[11] J. M. De Miranda,[1] L. De Paula,[2] W. De Silva,[57] P. De Simone,[18] D. Decamp,[4] M. Deckenhoff,[9] L. Del Buono,[8] N. Déléage,[4] D. Derkach,[55] O. Deschamps,[5] F. Dettori,[38] A. Di Canto,[38] H. Dijkstra,[38] S. Donleavy,[52] F. Dordei,[11] M. Dorigo,[39] A. Dosil Suárez,[37] D. Dossett,[48] A. Dovbnya,[43] K. Dreimanis,[52] G. Dujany,[54] F. Dupertuis,[39] P. Durante,[38] R. Dzhelyadin,[35] A. Dziurda,[26] A. Dzyuba,[30] S. Easo,[49,38] U. Egede,[53] V. Egorychev,[31] S. Eidelman,[34] S. Eisenhardt,[50] U. Eitschberger,[9] R. Ekelhof,[9] L. Eklund,[51,38] I. El Rifai,[5] Ch. Elsasser,[40] S. Ely,[59] S. Esen,[11] H.-M. Evans,[47] T. Evans,[55] A. Falabella,[14] C. Färber,[11] C. Farinelli,[41] N. Farley,[45] S. Farry,[52] RF Fay,[52] D. Ferguson,[50] V. Fernandez Albor,[37] F. Ferreira Rodrigues,[1] M. Ferro-Luzzi,[38] S. Filippov,[33] M. Fiore,[16,b] M. Fiorini,[16,b] M. Firlej,[27] C. Fitzpatrick,[38] T. Fiutowski,[27] M. Fontana,[10] F. Fontanelli,[19,j] R. Forty,[38] O. Francisco,[2] M. Frank,[38] C. Frei,[38] M. Frosini,[17,38,a] J. Fu,[21,38] E. Furfaro,[24,i] A. Gallas Torreira,[37] D. Galli,[14,h] S. Gallorini,[22] S. Gambetta,[19,j] M. Gandelman,[2] P. Gandini,[59] Y. Gao,[3] J. García Pardiñas,[37] J. Garofoli,[59] J. Garra Tico,[47] L. Garrido,[36] C. Gaspar,[38] R. Gauld,[55] L. Gavardi,[9] G. Gavrilov,[30] E. Gersabeck,[11] M. Gersabeck,[54] T. Gershon,[48] Ph. Ghez,[4] A. Gianelle,[22] S. Giani',[39] V. Gibson,[47] L. Giubega,[29] V. V. Gligorov,[38] C. Göbel,[60] D. Golubkov,[31] A. Golutvin,[53,31,38] A. Gomes,[1,k] H. Gordon,[38] C. Gotti,[20]

M. Grabalosa Gándara,[5] R. Graciani Diaz,[36] L. A. Granado Cardoso,[38] E. Graugés,[36] G. Graziani,[17] A. Grecu,[29] E. Greening,[55] S. Gregson,[47] P. Griffith,[45] L. Grillo,[11] O. Grünberg,[62] B. Gui,[59] E. Gushchin,[33] Yu. Guz,[35,38] T. Gys,[38] C. Hadjivasiliou,[59] G. Haefeli,[39] C. Haen,[38] S. C. Haines,[47] S. Hall,[53] B. Hamilton,[58] T. Hampson,[46] X. Han,[11] S. Hansmann-Menzemer,[11] N. Harnew,[55] S. T. Harnew,[46] J. Harrison,[54] J. He,[38] T. Head,[38] V. Heijne,[41] K. Hennessy,[52] P. Henrard,[5] L. Henry,[8] J. A. Hernando Morata,[37] E. van Herwijnen,[38] M. Heß,[62] A. Hicheur,[1] D. Hill,[55] M. Hoballah,[5] C. Hombach,[54] W. Hulsbergen,[41] P. Hunt,[55] N. Hussain,[55] D. Hutchcroft,[52] D. Hynds,[51] M. Idzik,[27] P. Ilten,[56] R. Jacobsson,[38] A. Jaeger,[11] J. Jalocha,[55] E. Jans,[41] P. Jaton,[39] A. Jawahery,[58] F. Jing,[3] M. John,[55] D. Johnson,[55] C. R. Jones,[47] C. Joram,[38] B. Jost,[38] N. Jurik,[59] M. Kaballo,[9] S. Kandybei,[43] W. Kanso,[6] M. Karacson,[38] T. M. Karbach,[38] S. Karodia,[51] M. Kelsey,[59] I. R. Kenyon,[45] T. Ketel,[42] B. Khanji,[20] C. Khurewathanakul,[39] S. Klaver,[54] K. Klimaszewski,[28] O. Kochebina,[7] M. Kolpin,[11] I. Komarov,[39] R. F. Koopman,[42] P. Koppenburg,[41,38] M. Korolev,[32] A. Kozlinskiy,[41] L. Kravchuk,[33] K. Kreplin,[11] M. Kreps,[48] G. Krocker,[11] P. Krokovny,[34] F. Kruse,[9] W. Kucewicz,[26,l] M. Kucharczyk,[20,26,38,f] V. Kudryavtsev,[34] K. Kurek,[28] T. Kvaratskheliya,[31] V. N. La Thi,[39] D. Lacarrere,[38] G. Lafferty,[54] A. Lai,[15] D. Lambert,[50] R. W. Lambert,[42] G. Lanfranchi,[18] C. Langenbruch,[48] B. Langhans,[38] T. Latham,[48] C. Lazzeroni,[45] R. Le Gac,[6] J. van Leerdam,[41] J.-P. Lees,[4] R. Lefèvre,[5] A. Leflat,[32] J. Lefrançois,[7] S. Leo,[23] O. Leroy,[6] T. Lesiak,[26] B. Leverington,[11] Y. Li,[3] T. Likhomanenko,[63] M. Liles,[52] R. Lindner,[38] C. Linn,[38] F. Lionetto,[40] B. Liu,[15] G. Liu,[38] S. Lohn,[38] I. Longstaff,[51] J. H. Lopes,[2] N. Lopez-March,[39] P. Lowdon,[40] H. Lu,[3] D. Lucchesi,[22,e] H. Luo,[50] A. Lupato,[22] E. Luppi,[16,b] O. Lupton,[55] F. Machefert,[7] I. V. Machikhiliyan,[31] F. Maciuc,[29] O. Maev,[30] S. Malde,[55] G. Manca,[15,m] G. Mancinelli,[6] J. Maratas,[5] J. F. Marchand,[4] U. Marconi,[14] C. Marin Benito,[36] P. Marino,[23,n] R. Märki,[39] J. Marks,[11] G. Martellotti,[25] A. Martens,[8] A. Martín Sánchez,[7] M. Martinelli,[41] D. Martinez Santos,[42] F. Martinez Vidal,[64] D. Martins Tostes,[2] A. Massafferri,[1] R. Matev,[38] Z. Mathe,[38] C. Matteuzzi,[20] A. Mazurov,[16,b] M. McCann,[53] J. McCarthy,[45] A. McNab,[54] R. McNulty,[12] B. McSkelly,[52] B. Meadows,[57] F. Meier,[9] M. Meissner,[11] M. Merk,[41] D. A. Milanes,[8] M.-N. Minard,[4] N. Moggi,[14] J. Molina Rodriguez,[60] S. Monteil,[5] M. Morandin,[22] P. Morawski,[27] A. Mordà,[6] M. J. Morello,[23,n] J. Moron,[27] A.-B. Morris,[50] R. Mountain,[59] F. Muheim,[50] K. Müller,[40] M. Mussini,[14] B. Muster,[39] P. Naik,[46] T. Nakada,[39] R. Nandakumar,[49] I. Nasteva,[2] M. Needham,[50] N. Neri,[21] S. Neubert,[38] N. Neufeld,[38] M. Neuner,[11] A. D. Nguyen,[39] T. D. Nguyen,[39] C. Nguyen-Mau,[39,o] M. Nicol,[7] V. Niess,[5] R. Niet,[9] N. Nikitin,[32] T. Nikodem,[11] A. Novoselov,[35] D. P. O'Hanlon,[48] A. Oblakowska-Mucha,[27] V. Obraztsov,[35] S. Oggero,[41] S. Ogilvy,[51] O. Okhrimenko,[44] R. Oldeman,[15,m] G. Onderwater,[65] M. Orlandea,[29] J. M. Otalora Goicochea,[2] P. Owen,[53] A. Oyanguren,[64] B. K. Pal,[59] A. Palano,[13,p] F. Palombo,[21,q] M. Palutan,[18] J. Panman,[38] A. Papanestis,[49,38] M. Pappagallo,[51] C. Parkes,[54] C. J. Parkinson,[9,45] G. Passaleva,[17] G. D. Patel,[52] M. Patel,[53] C. Patrignani,[19,j] A. Pazos Alvarez,[37] A. Pearce,[54] A. Pellegrino,[41] M. Pepe Altarelli,[38] S. Perazzini,[14,h] E. Perez Trigo,[37] P. Perret,[5] M. Perrin-Terrin,[6] L. Pescatore,[45] E. Pesen,[66] K. Petridis,[53] A. Petrolini,[19,j] E. Picatoste Olloqui,[36] B. Pietrzyk,[4] T. Pilař,[48] D. Pinci,[25] A. Pistone,[19] S. Playfer,[50] M. Plo Casasus,[37] F. Polci,[8] A. Poluektov,[48,34] E. Polycarpo,[2] A. Popov,[35] D. Popov,[10] B. Popovici,[29] C. Potterat,[2] E. Price,[46] J. Prisciandaro,[39] A. Pritchard,[52] C. Prouve,[46] V. Pugatch,[44] A. Puig Navarro,[39] G. Punzi,[23,r] W. Qian,[4] B. Rachwal,[26] J. H. Rademacker,[46] B. Rakotomiaramanana,[39] M. Rama,[18] M. S. Rangel,[2] I. Raniuk,[43] N. Rauschmayr,[38] G. Raven,[42] S. Reichert,[54] M. M. Reid,[48] A. C. dos Reis,[1] S. Ricciardi,[49] S. Richards,[46] M. Rihl,[38] K. Rinnert,[52] V. Rives Molina,[36] D. A. Roa Romero,[5] P. Robbe,[7] A. B. Rodrigues,[1] E. Rodrigues,[54] P. Rodriguez Perez,[54] S. Roiser,[38] V. Romanovsky,[35] A. Romero Vidal,[37] M. Rotondo,[22] J. Rouvinet,[39] T. Ruf,[38] F. Ruffini,[23] H. Ruiz,[36] P. Ruiz Valls,[64] J. J. Saborido Silva,[37] N. Sagidova,[30] P. Sail,[51] B. Saitta,[15,m] V. Salustino Guimaraes,[2] C. Sanchez Mayordomo,[64] B. Sanmartin Sedes,[37] R. Santacesaria,[25] C. Santamarina Rios,[37] E. Santovetti,[24,i] A. Sarti,[18,s] C. Satriano,[25,c] A. Satta,[24] D. M. Saunders,[46] M. Savrie,[16,b] D. Savrina,[31,32] M. Schiller,[42] H. Schindler,[38] M. Schlupp,[9] M. Schmelling,[10] B. Schmidt,[38] O. Schneider,[39] A. Schopper,[38] M.-H. Schune,[7] R. Schwemmer,[38] B. Sciascia,[18] A. Sciubba,[25] M. Seco,[37] A. Semennikov,[31] I. Sepp,[53] N. Serra,[40] J. Serrano,[6] L. Sestini,[22] P. Seyfert,[11] M. Shapkin,[35] I. Shapoval,[16,43,b] Y. Shcheglov,[30] T. Shears,[52] L. Shekhtman,[34] V. Shevchenko,[63] A. Shires,[9] R. Silva Coutinho,[48] G. Simi,[22] M. Sirendi,[47] N. Skidmore,[46] T. Skwarnicki,[59] N. A. Smith,[52] E. Smith,[55,49] E. Smith,[53] J. Smith,[47] M. Smith,[54] H. Snoek,[41] M. D. Sokoloff,[57] F. J. P. Soler,[51] F. Soomro,[39] D. Souza,[46] B. Souza De Paula,[2] B. Spaan,[9] A. Sparkes,[50] P. Spradlin,[51] S. Sridharan,[38] F. Stagni,[38] M. Stahl,[11] S. Stahl,[11] O. Steinkamp,[40] O. Stenyakin,[35] S. Stevenson,[55] S. Stoica,[29] S. Stone,[59] B. Storaci,[40] S. Stracka,[23,38] M. Straticiuc,[29] U. Straumann,[40] R. Stroili,[22] V. K. Subbiah,[38] L. Sun,[57] W. Sutcliffe,[53] K. Swientek,[27] S. Swientek,[9] V. Syropoulos,[42] M. Szczekowski,[28] P. Szczypka,[39,38] D. Szilard,[2] T. Szumlak,[27] S. T'Jampens,[4] M. Teklishyn,[7] G. Tellarini,[16,b] F. Teubert,[38] C. Thomas,[55] E. Thomas,[38] J. van Tilburg,[41] V. Tisserand,[4] M. Tobin,[39] S. Tolk,[42] L. Tomassetti,[16,b] D. Tonelli,[38]

S. Topp-Joergensen,[55] N. Torr,[55] E. Tournefier,[4] S. Tourneur,[39] M. T. Tran,[39] M. Tresch,[40] A. Tsaregorodtsev,[6] P. Tsopelas,[41] N. Tuning,[41] M. Ubeda Garcia,[38] A. Ukleja,[28] A. Ustyuzhanin,[63] U. Uwer,[11] V. Vagnoni,[14] G. Valenti,[14] A. Vallier,[7] R. Vazquez Gomez,[18] P. Vazquez Regueiro,[37] C. Vázquez Sierra,[37] S. Vecchi,[16] J. J. Velthuis,[46] M. Veltri,[17,t] G. Veneziano,[39] M. Vesterinen,[11] B. Viaud,[7] D. Vieira,[2] M. Vieites Diaz,[37] X. Vilasis-Cardona,[36,g] A. Vollhardt,[40] D. Volyanskyy,[10] D. Voong,[46] A. Vorobyev,[30] V. Vorobyev,[34] C. Voß,[62] H. Voss,[10] J. A. de Vries,[41] R. Waldi,[62] C. Wallace,[48] R. Wallace,[12] J. Walsh,[23] S. Wandernoth,[11] J. Wang,[59] D. R. Ward,[47] N. K. Watson,[45] D. Websdale,[53] M. Whitehead,[48] J. Wicht,[38] D. Wiedner,[11] G. Wilkinson,[55] M. P. Williams,[45] M. Williams,[56] F. F. Wilson,[49] J. Wimberley,[58] J. Wishahi,[9] W. Wislicki,[28] M. Witek,[26] G. Wormser,[7] S. A. Wotton,[47] S. Wright,[47] S. Wu,[3] K. Wyllie,[38] Y. Xie,[61] Z. Xing,[59] Z. Xu,[39] Z. Yang,[3] X. Yuan,[3] O. Yushchenko,[35] M. Zangoli,[14] M. Zavertyaev,[10,u] L. Zhang,[59] W. C. Zhang,[12] Y. Zhang,[3] A. Zhelezov,[11] A. Zhokhov,[31] L. Zhong[3] and A. Zvyagin[38]

(LHCb Collaboration)

[1]*Centro Brasileiro de Pesquisas Físicas (CBPF), Rio de Janeiro, Brazil*
[2]*Universidade Federal do Rio de Janeiro (UFRJ), Rio de Janeiro, Brazil*
[3]*Center for High Energy Physics, Tsinghua University, Beijing, China*
[4]*LAPP, Université de Savoie, CNRS/IN2P3, Annecy-Le-Vieux, France*
[5]*Clermont Université, Université Blaise Pascal, CNRS/IN2P3, LPC, Clermont-Ferrand, France*
[6]*CPPM, Aix-Marseille Université, CNRS/IN2P3, Marseille, France*
[7]*LAL, Université Paris-Sud, CNRS/IN2P3, Orsay, France*
[8]*LPNHE, Université Pierre et Marie Curie, Université Paris Diderot, CNRS/IN2P3, Paris, France*
[9]*Fakultät Physik, Technische Universität Dortmund, Dortmund, Germany*
[10]*Max-Planck-Institut für Kernphysik (MPIK), Heidelberg, Germany*
[11]*Physikalisches Institut, Ruprecht-Karls-Universität Heidelberg, Heidelberg, Germany*
[12]*School of Physics, University College Dublin, Dublin, Ireland*
[13]*Sezione INFN di Bari, Bari, Italy*
[14]*Sezione INFN di Bologna, Bologna, Italy*
[15]*Sezione INFN di Cagliari, Cagliari, Italy*
[16]*Sezione INFN di Ferrara, Ferrara, Italy*
[17]*Sezione INFN di Firenze, Firenze, Italy*
[18]*Laboratori Nazionali dell'INFN di Frascati, Frascati, Italy*
[19]*Sezione INFN di Genova, Genova, Italy*
[20]*Sezione INFN di Milano Bicocca, Milano, Italy*
[21]*Sezione INFN di Milano, Milano, Italy*
[22]*Sezione INFN di Padova, Padova, Italy*
[23]*Sezione INFN di Pisa, Pisa, Italy*
[24]*Sezione INFN di Roma Tor Vergata, Roma, Italy*
[25]*Sezione INFN di Roma La Sapienza, Roma, Italy*
[26]*Henryk Niewodniczanski Institute of Nuclear Physics Polish Academy of Sciences, Kraków, Poland*
[27]*AGH - University of Science and Technology, Faculty of Physics and Applied Computer Science, Kraków, Poland*
[28]*National Center for Nuclear Research (NCBJ), Warsaw, Poland*
[29]*Horia Hulubei National Institute of Physics and Nuclear Engineering, Bucharest-Magurele, Romania*
[30]*Petersburg Nuclear Physics Institute (PNPI), Gatchina, Russia*
[31]*Institute of Theoretical and Experimental Physics (ITEP), Moscow, Russia*
[32]*Institute of Nuclear Physics, Moscow State University (SINP MSU), Moscow, Russia*
[33]*Institute for Nuclear Research of the Russian Academy of Sciences (INR RAN), Moscow, Russia*
[34]*Budker Institute of Nuclear Physics (SB RAS) and Novosibirsk State University, Novosibirsk, Russia*
[35]*Institute for High Energy Physics (IHEP), Protvino, Russia*
[36]*Universitat de Barcelona, Barcelona, Spain*
[37]*Universidad de Santiago de Compostela, Santiago de Compostela, Spain*
[38]*European Organization for Nuclear Research (CERN), Geneva, Switzerland*
[39]*Ecole Polytechnique Fédérale de Lausanne (EPFL), Lausanne, Switzerland*
[40]*Physik-Institut, Universität Zürich, Zürich, Switzerland*
[41]*Nikhef National Institute for Subatomic Physics, Amsterdam, The Netherlands*
[42]*Nikhef National Institute for Subatomic Physics and VU University Amsterdam, Amsterdam, The Netherlands*
[43]*NSC Kharkiv Institute of Physics and Technology (NSC KIPT), Kharkiv, Ukraine*

[44]*Institute for Nuclear Research of the National Academy of Sciences (KINR), Kyiv, Ukraine*
[45]*University of Birmingham, Birmingham, United Kingdom*
[46]*H.H. Wills Physics Laboratory, University of Bristol, Bristol, United Kingdom*
[47]*Cavendish Laboratory, University of Cambridge, Cambridge, United Kingdom*
[48]*Department of Physics, University of Warwick, Coventry, United Kingdom*
[49]*STFC Rutherford Appleton Laboratory, Didcot, United Kingdom*
[50]*School of Physics and Astronomy, University of Edinburgh, Edinburgh, United Kingdom*
[51]*School of Physics and Astronomy, University of Glasgow, Glasgow, United Kingdom*
[52]*Oliver Lodge Laboratory, University of Liverpool, Liverpool, United Kingdom*
[53]*Imperial College London, London, United Kingdom*
[54]*School of Physics and Astronomy, University of Manchester, Manchester, United Kingdom*
[55]*Department of Physics, University of Oxford, Oxford, United Kingdom*
[56]*Massachusetts Institute of Technology, Cambridge, Massachusetts 02139, USA*
[57]*University of Cincinnati, Cincinnati, Ohio 45221, USA*
[58]*University of Maryland, College Park, Maryland 20742, USA*
[59]*Syracuse University, Syracuse, New York 13244, USA*
[60]*Pontifícia Universidade Católica do Rio de Janeiro (PUC-Rio), Rio de Janeiro, Brazil*
(associated with Universidade Federal do Rio de Janeiro (UFRJ), Rio de Janeiro, Brazil)
[61]*Institute of Particle Physics, Central China Normal University, Wuhan, Hubei, China*
(associated with Center for High Energy Physics, Tsinghua University, Beijing, China)
[62]*Institut für Physik, Universität Rostock, Rostock, Germany*
(associated with Physikalisches Institut, Ruprecht-Karls-Universität Heidelberg, Heidelberg, Germany)
[63]*National Research Centre Kurchatov Institute, Moscow, Russia*
(associated with Institute of Theoretical and Experimental Physics (ITEP), Moscow, Russia)
[64]*Instituto de Fisica Corpuscular (IFIC), Universitat de Valencia-CSIC, Valencia, Spain*
(associated with Universitat de Barcelona, Barcelona, Spain)
[65]*KVI - University of Groningen, Groningen, The Netherlands*
(associated with Nikhef National Institute for Subatomic Physics, Amsterdam, The Netherlands)
[66]*Celal Bayar University, Manisa, Turkey*
(associated with European Organization for Nuclear Research (CERN), Geneva, Switzerland)

[a]Also at Università di Firenze, Firenze, Italy.
[b]Also at Università di Ferrara, Ferrara, Italy.
[c]Also at Università della Basilicata, Potenza, Italy.
[d]Also at Università di Modena e Reggio Emilia, Modena, Italy.
[e]Also at Università di Padova, Padova, Italy.
[f]Also at Università di Milano Bicocca, Milano, Italy.
[g]Also at LIFAELS, La Salle, Universitat Ramon Llull, Barcelona, Spain.
[h]Also at Università di Bologna, Bologna, Italy.
[i]Also at Università di Roma Tor Vergata, Roma, Italy.
[j]Also at Università di Genova, Genova, Italy.
[k]Also at Universidade Federal do Triângulo Mineiro (UFTM), Uberaba-MG, Brazil.
[l]Also at AGH - University of Science and Technology, Faculty of Computer Science, Electronics and Telecommunications, Kraków, Poland.
[m]Also at Università di Cagliari, Cagliari, Italy.
[n]Also at Scuola Normale Superiore, Pisa, Italy.
[o]Also at Hanoi University of Science, Hanoi, Viet Nam.
[p]Also at Università di Bari, Bari, Italy.
[q]Also at Università degli Studi di Milano, Milano, Italy.
[r]Also at Università di Pisa, Pisa, Italy.
[s]Also at Università di Roma La Sapienza, Roma, Italy.
[t]Also at Università di Urbino, Urbino, Italy.
[u]Also at P.N. Lebedev Physical Institute, Russian Academy of Science (LPI RAS), Moscow, Russia.